Carbon-13 Chemical-Shift Tensors in Polycyclic Aromatic Compounds: Fluoranthene and Decacyclene

Dewey H. Barich,[†] Jian Zhi Hu,[†] Ronald J. Pugmire,[‡] and David M. Grant*[,†]

Departments of Chemistry and Chemical and Fuels Engineering, University of Utah, Salt Lake City, Utah 84112

Received: December 19, 2001; In Final Form: April 23, 2002

The principal values of the chemical-shift tensor (CST) for fluoranthene and decacyclene have been determined with the FIREMAT experiment to study the effects of ring strain associated with fusing five- and six-member rings. The measured CST principal values of each molecule are compared to density functional theory predictions. The results are discussed in terms of previously determined chemical shift data of related molecules. The effects of nonplanar distortions and substitution are separated through computational efforts. A correlation between the computed and the experimental data results in an RMS of 5.6 ppm, a value that is slightly larger than is typically found in other polycyclic aromatic hydrocarbons.

Introduction

The measurement of ^{13}C chemical-shift tensors (CSTs) of polycyclic aromatic hydrocarbons (PAHs) has received considerable attention in recent years.[1−7] Challenges to measuring CSTs in aromatic microcrystalline powders include spectral complexity due to the spinning sideband patterns, the relatively close isotropic chemical shifts of the various carbons in the molecule (typically 120−140 ppm), and coincidental overlap of equivalent molecular positions in crystallographically inequivalent sites. Spectral complexity is reduced in this work by application of the FIREMAT experiment, a two-dimensional (2D) magic angle turning (MAT) experiment that isolates individual sideband patterns associated with different isotropic chemical shifts.[8] Recent advances in such methods have made possible the isolation of several dozen sideband patterns from a composite spectrum.[8] Line broadening due to magnetic susceptibility anisotropy in the microcrystalline aromatic samples provides another challenge to accurate determination of the CST principal values. This anisotropic interaction is manifest as inhomogeneous broadening in the spectra of the two compounds studied. In this report, inhomogeneous broadening, which does not satisfy the criteria for applying TIGER processing,[9] is modeled by directly fitting the 2D FID with model FIDs that include inhomogeneous broadening, thereby circumventing the TIGER processing typically used in FIREMAT experiments.

The present work reports the CSTs for microcrystalline samples of fluoranthene (**1**) and decacyclene (**2**), shown below. Fluoranthene crystallizes[10] in the $P2_1/n$ space group with two distinct molecules per asymmetric crystallographic unit and thus eight molecules per unit cell (Figure 1). Decacyclene may be viewed as a substituted fluoranthene. Indeed, its systematic IUPAC name is diacenaphtho[1,2-j,1′,2′-l]fluoranthene. Decacyclene crystallizes[11] in the $C222_1$ space group with one-half of a molecule in an asymmetric unit and four molecules in the unit cell (Figure 2).

Fluoranthene, **1**

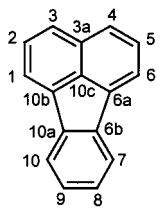

Decacyclene, **2**

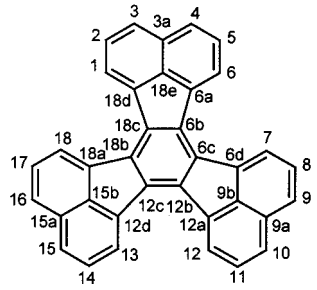

There are few literature examples of ^{13}C CST principal values for PAHs that contain five-member rings.[3,4,7,12,13] These compounds are of interest because of the bond strain associated with the fusion of five- and six-member rings and the associated nonplanar distortions that frequently occur. Such data is important to the study of carbonaceous materials such as coals and soots, which are complicated mixtures of a wide variety of PAHs.[14−16] Spectral analysis of such materials often employs data from model compounds. This work thus increases the number of model compound examples and contributes toward a better understanding of the ring strain effects on ^{13}C CSTs.

In addition to containing a five-member ring, **2** exhibits another interesting structural feature. Proximate hydrogen atoms of adjacent naphthalene moieties lie closer than the sum of their van der Waals radii. The forces imposed by this steric interaction twist the naphthalene moieties out of the mean molecular plane, resulting in a propeller-shaped structure. The C_2 symmetry of **2** in the crystal dictates that there be one unique naphthalene moiety and two symmetry-related ones. The X-ray data indicate that the unique one is twisted 7.8° from the central benzene ring plane. The other two are each twisted 9.3° from the central benzene ring plane, thus completing the propeller-like structure. Barnett et al.[17] recently reported a simple means of predicting the conformation (D_3 vs C_2) of highly symmetric but crowded PAHs based upon the central ring's electronic structure. The nonplanar distortion in **2** provides an opportunity to better understand such effects on CSTs, for which a paucity of data exist. One of the few reports[4] of a nonplanar PAH is corannulene, dibenzo[*ghi*,*mno*]fluoranthene.

* To whom correspondence should be addressed.
[†] Department of Chemistry.
[‡] Department Chemical and Fuels Engineering.

10.1021/jp0146162 CCC: $22.00
Published on Web 06/18/2002

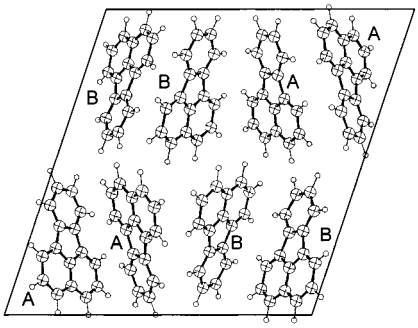

Figure 1. Simplified representation of the monoclinic fluoranthene crystal viewed along the crystallographic *b* axis. The two distinct molecules are labeled A and B. One crystallographic inversion center is located at the center of the unit cell. The two cases of adjacent A and B molecules near the middle of the box (one pair above and one below) each constitute a whole asymmetric unit, which is the system (when isolated from the rest of the lattice) used for the quantum mechanical calculations. The four corner molecules each constitute one-half of an asymmetric unit and pair with a molecule that lies outside the unit cell.

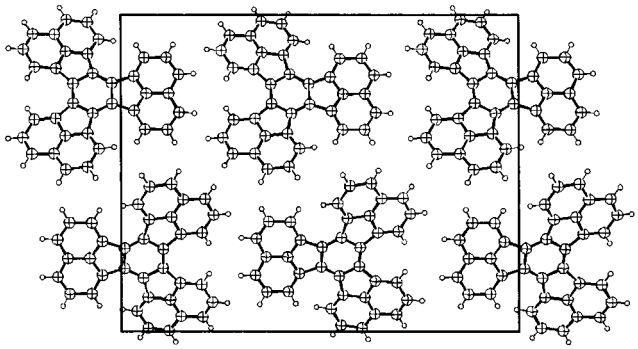

Figure 2. Simplified representation of the orthorhombic decacyclene crystal viewed along the crystallographic *a* axis. The *b* axis is horizonatal, and the *c* axis is vertical. The asymmetric unit is one-half of one molecule divided along a horizontal axis.

Methods

Experimental. Both **1** and **2** were obtained from Aldrich and used without further purification. Both molecules have only one known crystal structure, and these were verified by X-ray powder diffraction. All NMR experiments were carried out on a CMX-200 spectrometer operating with a Larmor frequency of 50.3 MHz for ^{13}C and 200.0 MHz for ^{1}H. To enhance signal intensity, cross polarization (CP) was used in all experiments.[18] Proton decoupling was carried out at a field strength of approximately 64 kHz. A constant time condition was used for **1** in which a recycle time of 180 s yielded optimal signal-to-noise for a given experiment time in a CP FIREMAT experiment.[8] The $\pi/2$ pulse widths were 3.8 and 4.0 μs for the ^{1}H and ^{13}C channels, respectively. A contact time of 4.0 ms was used. The spinning speed was 800 Hz. There were 48 data points collected during each rotor cycle. The spectral widths were 38 400 and 6400 Hz for the acquisition and evolution dimensions, respectively. A total of 914 data points were collected in each of eight evolution increments. Each evolution FID is the sum of 768 transients. A dipolar dephased (DD) FIREMAT[8] was then carried out on the sample with a total dephasing time of 100 μs. All other spectral conditions were identical to the CP FIREMAT.

The ^{1}H T_1 of **2** was determined by saturation recovery to be 31 s. A standard CP FIREMAT experiment was performed at a spin rate of 960 Hz. The spectral widths were 46 080 and 7680 Hz for the acquisition and evolution dimensions, respectively. There were 48 data points collected during each rotor cycle. A total of 512 data points were collected in each of eight evolution increments. Each evolution FID was the sum of 1536 transients. A dipolar dephased FIREMAT experiment was performed under identical conditions as described for the DD FIREMAT of **1** with 192 transients collected for each evolution FID. Each FID consisted of 4088 data points. The contact time was increased from 4.0 to 8.5 ms. Data processing and spectral analysis was performed on a Sun computer.

Theoretical. All calculations were performed with Gaussian 98.[19] All basis sets used spherical Gaussians. The chemical shielding calculations employed the gauge-including atomic orbitals (GIAO) ansatz.[20−22] The diffraction determined positions (neutron[10] for **1** and X-ray[11] for **2**) for the carbon atoms were retained while the proton positions were optimized at the B3LYP/D95* level of theory.[23−25] The model employed for **1** included both molecules in the crystallographic asymmetric unit (Figure 1). The model for **2** was one molecule isolated from the lattice (Figure 2). This model of **2** is composed of two crystallographic asymmetric units whose intrinsic C_2 symmetry was used in the calculations.

There are two primary structural differences between **1** and **2**, substitution and twist, whose separate effects cannot be experimentally isolated. Hence, a theoretical model that allows isolation of these two effects is needed. This theoretical model is a twisted fluoranthene that differs from **1** only by a twist and differs from **2** only by substitution of two naphthalene moieties. Such a model is constructed by removing two of the three naphthalene moieties from **2**. Because **2** contains three naphthalene moieites, it is possible to create three different twisted fluoranthene models; however, as two of the naphthalene moieties are symmetry related, only two models need to be constructed, and their results averaged in a 2:1 ratio. The 2-fold contributor to this average consists of the central benzene ring of **2** and one of its symmetry-related naphthalene moieties. The other contributor consists of the central benzene ring and the unique naphthalene moiety. After removing the naphthalenes, the central benzene ring's valence was filled with protons whose positions were optimized at the B3LYP/D95* level of theory.[23−25]

The chemical shielding tensors were then calculated at the GIAO-B3PW91/D95** level of theory,[26−28] for **1**, **2**, and each of the twisted fluoranthene models. The B3PW91 level of theory yielded a smaller RMS value than B3LYP for the correlation of theory vs experiment in a study of biphenylene.[2] The results of the two twisted fluoranthene molecules were averaged together in a 2:1 ratio.

Because of limited spectral resolution, it was necessary to average some calculated principal values before comparing them with the experimental data. Some averaging involved only equivalent molecular positions that are crystallographically distinct (e.g., C3 and C4 from each molecule of **1** in the model), whereas some also involved molecular positions that were experimentally indistinguishable (e.g., in **1**, C1 and C6 were averaged with C7 and C10). In **1**, the ideal C_{2v} symmetry is not observed in either molecule in the crystal; thus, those carbons that have symmetry partners in the ideal case are distinguishable in the theoretical calculations and are treated as such in the following description. The calculated results of both molecules of **1** from the theory model were averaged together as follows: (C1, C6, C7, C10), (C2, C5, C8, C9), and (C3, C4). As all of the quaternary molecular positions were resolved in the experiment, they are averaged only over the contributions from the corresponding nuclei in the two molecules. For **2**, seven molecular groupings are resolved. The observed C_2 symmetry

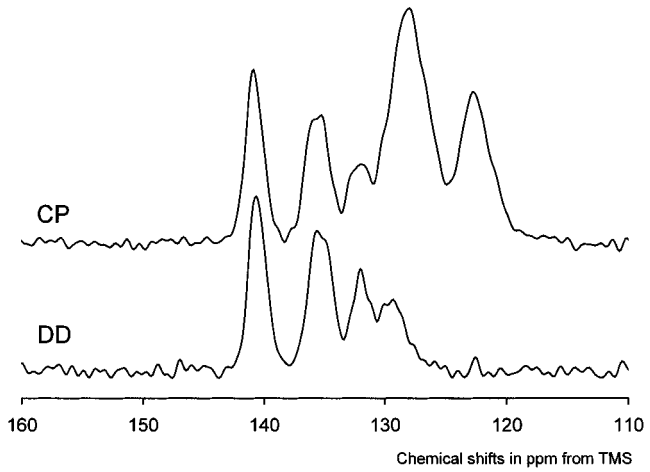

Figure 3. FIREMAT guide spectra of **1**. The DD spectrum shows the quaternary peak located at 129.4 ppm that is resolved only via dipolar dephasing because of accidental overlap with protonated carbon peaks.

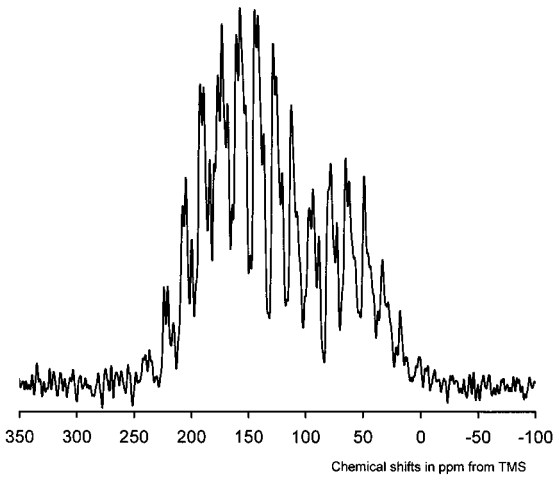

Figure 4. First increment of the CP FIREMAT of **1**.

of **2** in the crystal results in two naphthalene moieties being equivalent. The C_2 axis passes through C3a and C18e; thus, although C9a and C15a are equivalent in the crystal, they are distinct from C3a. All three of these positions, however, are inseparable in the experimental data, and thus, their calculated values were averaged prior to comparison with the experimental data. The calculated results for the following carbon sets were averaged: (C1, C6, C7, C12, C13, C18), (C2, C5, C8, C11, C14, C17), (C3, C4, C9, C10, C15, C16), (C6a, C6d, C12a, C12d, C18a, C18d), (C6b, C6c, C12b, C12c, C18b, C18c), (C3a, C9a, C15a), and (C9b, C15b, C18e).

Once the averaging was completed, the calculated shieldings were plotted against the experimental shifts. The GIAO-B3PW91/D95** shieldings (σ) were converted to the chemical shift scale (δ) with the best-fit line, $\sigma_{calc} = -0.97\ (\pm 0.02)\ \delta_{calc} + 188\ (\pm 3)$. Uncertainties for the slope and intercept are given at the 95% confidence interval.

Chemical Shift Assignments. A modified version (that uses only principal values not full tensors) of a previously reported assignment procedure[29] was used. Both the averaged calculated principal shielding values and the experimental CST principal values were converted to the icosahedral tensor representation.[30] All possible permutational assignments were then considered (for N tensors there are $N!$ possibilities), and the variance of the least-squares fit of the computed shieldings vs the experimental shifts is calculated for each proposed assignment scheme. The assignment scheme that yields the smallest variance is taken as the most probable assignment. Each alternate assignment's variance is compared to the optimal variance in an F test to assign a confidence level at which the alternate assignment could be neglected relative to the best overall assignment. The experimental values from the dipolar dephased experiments allow assignment of all four quaternary peaks of each molecule. The same procedure was applied to the protonated carbon data. Because of the limited resolution arising from susceptibility broadening, the predicted values of the CH carbons of **1** were averaged prior to application of this assignment scheme because only two peaks associated with CH carbons were resolved in the experiment. In **2**, the assignment process involved all three resolved CH peaks.

Results

Spectral Analysis. The guide spectrum from the CP FIREMAT of **1** is shown at the top of Figure 3 to aid in describing the fitting process. The data fitting was performed directly on the 2D data set (vide supra). Figure 4 shows the first increment of the 5π data set of **1**. Subsequent increments lack aesthetic appeal because of the phase-encoded nature of the experiment (i.e., all peaks cannot be properly phased simultaneously). The large line widths and small isotropic chemical shift range in the spectra give rise to only five resolved peaks in the guide spectrum. Further insight was achieved through additional experimentation and data analysis. One step was to acquire the DD spectrum, whose guide spectrum is shown at the bottom of Figure 3. Note that the lowest frequency quaternary line (129.4 ppm, DD spectrum) is obscured by accidental overlap with the CH carbons centered at ca. 127.7 ppm in the CP spectrum.

The two highest frequency lines (140.8 and 135.5 ppm) are sufficiently resolved to be analyzed in both the CP and DD FIREMAT spectra and yield indistinguishable results. The other two quaternary lines, centered at 132.0 and 129.4 ppm, are better resolved in the DD spectrum. The CST principal values derived from the DD FIREMAT data for these signals are used in the analysis of the CP FIREMAT spectrum to facilitate a more accurate determination of the CST principal values for the protonated carbons. The two CH peak intensities have a 3:2 ratio, which accounts for all five protonated carbon positions in **1**. Inspection of the solution state isotropic shifts[31,32] of the CH carbons show that the C1 and C7 carbons have similar isotropic shifts (122.9 and 120.7 ppm, respectively) and that the C2, C3, and C8 carbons have similar shifts (128.5, 127.3, and 128.3 ppm, respectively). Given the increased line widths in the solid-state NMR spectra of **1**, as well as allowing for modest changes in isotropic shifts between solution and solid phases, it is reasonable to expect that the 3:2 ratio of these two CH peaks corresponds to an overlap of the C2, C3, and C8 peaks and overlap of the C1 and C7 positions, respectively. The peak centered at 127.7 ppm was fit in a 2:1 ratio to two tensors whose resulting principal values differ by more than twice the anticipated errors, lending confidence to the multitensor determination. Consequently, seven of nine molecular positions were resolved in the experimental work.

Spectral analysis of **2** was similar to that of **1**. There is also overlap of a quaternary carbon and a protonated carbon signal. The principal values for the quaternary peak with isotropic shift of 128.7 ppm were determined from the DD spectrum. Those values were used in fitting the protonated carbons in the CP FIREMAT data as described above for **1**. The three protonated carbon peaks were analyzed with relative ease because there is some isotropic resolution, as can be seen in the guide spectrum

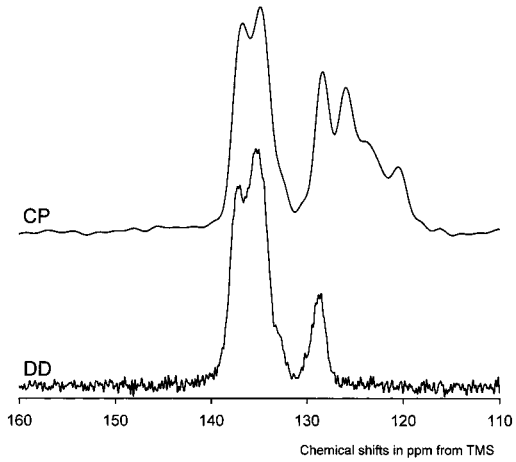

Figure 5. FIREMAT guide spectra of **2**. The DD spectrum shows the quaternary peak located at 128.7 ppm that is resolved only via dipolar dephasing because of accidental overlap with protonated carbon peaks.

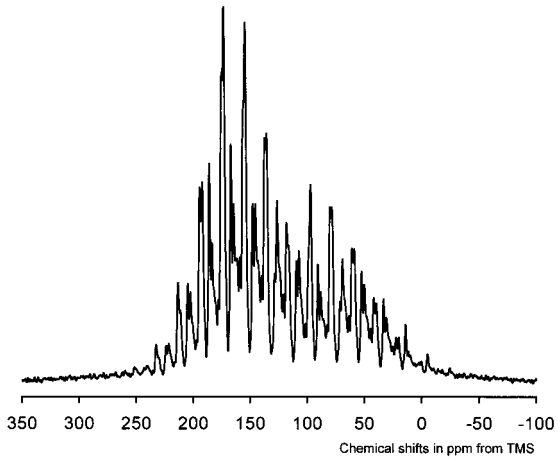

Figure 6. First increment of the CP FIREMAT of **2**.

of **2** in Figure 5. As with **1**, the FIREMAT data of **2** were directly fit from the 2D FID rather than by TIGER processing (Figure 6); however, the guide spectra are included once again for pedagogical reasons. The improved resolution found in this guide spectrum relative to **1** is partly due to the fact that **2** has only three nonequivalent protonated carbon positions in the molecule, whereas **1** has five. It was nevertheless necessary to constrain these three protonated peaks to a 1:1:1 intensity ratio in the data analysis. The most difficult fitting aspect of the spectrum of **2** involved the remaining three quaternary peaks. The guide spectrum shows only two well resolved peaks at frequencies higher than 128.7 ppm (with a low-frequency shoulder); however, there are a total of four quaternary molecular positions in **2**. The shoulder is assumed to be the fourth peak with an isotropic shift of ca. 134.1 ppm. It is barely resolved in the isotropic dimension of the FIREMAT spectrum because of the relatively large line widths. Moreover, this shoulder has only one-half the relative intensity of the other two peaks in this spectral region. The principal values of this peak could nevertheless be reliably determined because the near axial symmetry of this tensor is considerably different than that of the other overlapping peak thereby enabling signal separation.

Discussion

Bridgehead Carbons. Given that both **1** and **2** contain naphthalene moieties, it is natural to compare their CSTs with those of naphthalene for two reasons. First, naphthalene is the simplest aromatic molecule containing bridgehead carbons, thus providing a useful "baseline". Second, very accurate single crystal NMR data have previously been reported for naphthalene.[33] In naphthalene, the CST for the bridgehead carbon is nearly axially symmetric (two principal values are nearly identical), e.g., $|\delta_{11}-\delta_{22}| \approx 7$ ppm. The C9b position in **2** is almost exactly axially symmetric (Table 1), whereas the other bridgehead carbons (C3a of both molecules and C10c of **1**) also exhibit axial character although their acentricities are less than that found in naphthalene. The δ_{33} principal value for C3a in both molecules is negative, which is quite typical for this carbon type.

TABLE 1: Chemical-Shift Tensor Principal Values Determined by the FIREMAT Experiment

	IUPAC	δ_{11} ppm	δ_{22} ppm	δ_{33} ppm	δ_{iso} ppm	δ_{span}[a] ppm	δ_{acen}[b] ppm
1	1,7	208.8	149.3	9.5	122.5	199.2	40.1
	2,8	228.9	143.5	11.9	128.1	217.0	23.1
	3	217.8	140.7	20.8	126.5	197.0	21.3
	3a	202.6	188.4	−3.0	129.4	205.6	88.6
	6a	222.1	154.2	29.7	135.3	192.4	28.4
	6b	226.6	160.4	34.6	140.5	191.9	29.8
	10c	203.5	182.5	10.1	132.0	193.4	75.7
2	1	208.0	156.5	−3.4	120.4	211.4	54.2
	2	224.7	139.7	13.4	125.9	211.3	20.6
	3	209.9	142.9	18.7	123.8	191.2	28.6
	3a	207.2	190.1	−11.1	128.7	218.3	92.0
	6a	226.0	161.0	24.6	137.2	201.4	35.7
	6b	206.0	161.3	38.4	135.2	167.5	39.0
	9b	200.4	199.4	2.5	134.1	198.0	98.0

[a] $\delta_{span} = \delta_{11} - \delta_{33}$. [b] $\delta_{acentricity} = \delta_{22} - (\delta_{11} + \delta_{33})/2$.

TABLE 2: Chemical-Shift Tensor Principal Values Calculated at GIAO-B3PW91/D95**

	IUPAC	δ_{11} ppm	δ_{22} ppm	δ_{33} ppm	δ_{iso} ppm	δ_{span}[a] ppm	δ_{acen}[b] ppm
1	1,7	215.5	147.8	1.9	121.7	213.6	39.2
	2,8	231.5	139.0	11.2	127.2	220.3	17.6
	3	221.7	136.3	15.2	124.4	206.4	17.8
	3a	197.2	190.4	−19.4	122.7	216.6	101.5
	6a	219.0	158.9	29.9	135.9	189.1	34.4
	6b	220.2	159.9	33.7	138.0	186.5	33.0
	10c	198.4	191.1	4.7	131.4	193.7	89.5
2	1	210.2	151.7	6.6	122.9	203.6	43.3
	2	228.1	135.3	12.4	125.3	215.7	15.1
	3	218.9	138.5	16.9	124.7	202.0	20.6
	3a	198.1	195.1	−15.8	125.8	214.0	104.0
	6a	223.1	165.4	29.7	139.4	193.4	39.0
	6b	203.1	162.1	51.9	139.1	151.2	34.6
	9b	201.6	198.0	10.4	136.6	191.2	92.0

[a] $\delta_{span} = \delta_{11} - \delta_{33}$. [b] $\delta_{acentricity} = \delta_{22} - (\delta_{11} + \delta_{33})/2$.

Effects of Five-Member Rings. The δ_{33} CST principal values of the quaternary carbons that are part of the five-member rings, i.e., C6a, C6b, and C10c in **1** and C6a, C6b, and C9b in **2**, appear at higher frequency than analogous principal values in most other PAH compounds. This shift to higher frequency due to ring strain has previously been observed in several cases including corannulene[4] and biphenylene.[2] The carbons in **1** and **2** confirm this feature. The strain imposed on carbons C6a and C6b for both molecules has shifted the δ_{33} values (Table 1) to higher frequency relative to the same value for perylene's C6a (ca. 13.0 ppm), which is a component of a six-member ring. Even the δ_{33} values at the inner condensed positions in **1** (C10c, 10.1 ppm) and **2** (C9b, 2.5 ppm) are at higher frequency than the corresponding position in naphthalene (−5.9 ppm). A few literature examples[2,4,6,7,12,33] are tabulated in Table 3 for

TABLE 3. Selected Literature Examples of Chemical-Shift Tensor Principal Values

	molecule	IUPAC	δ_{11} ppm	δ_{22} ppm	δ_{33} ppm	δ_{iso} ppm	δ_{span}[a] ppm	δ_{acen}[b] ppm
no	acenaphthene	5a	201	199	−3	132	205	100
ring	corrannulene	2a	214	189	−10	131	224	87
strain	naphthalene	4a	209	202	−6	135	215	101
	perylene	3a	204	202	−3	134	206	102
	perylene	9b	195	193	−3	128	198	97
ring	acenaphthene	2a	238	170	37	148	201	33
strain	acenaphthene	8b	212	195	13	140	199	82
	biphenylene	4a	246	155	55	152	191	5
	corrannulene	10b	224	177	6	136	218	62
	perylene	6a	219	161	13	131	206	44
	pyracene	2a	226	166	36	143	190	35
	pyracene	8b	202	192	24	139	178	79

[a] $\delta_{span} = \delta_{11} - \delta_{33}$. [b] $\delta_{acentricity} = \delta_{22} - (\delta_{11} + \delta_{33})/2$.

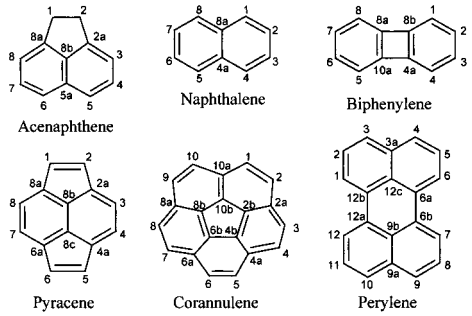

Figure 7. Structures of representative PAHs whose CST principal values are tabulated in Table 3 for discussion purposes.

comparison to the current data. The structures of these compounds are shown in Figure 7.

Effects of Nonplanar Twisting. Ring strain is not the only structural feature that could affect tensor values. A different source of strain is nonplanar distortions (twists) that reduce the $\pi-\pi$ overlap between adjacent sp^2 carbons. The CSTs of **2** reflect the twist of the planar naphthalene moieties relative to the central benzene ring. The effects of the twist cannot be isolated based on the experimental data because the addition of the naphthalene moieties that cause the twists also introduces substitution effects on the CSTs of the central benzene ring. Fortunately, theoretical work allows separation of the twist and substitution effects by constructing a twisted fluoranthene model and computing its CSTs. Comparison of the CST principal values of this twisted fluoranthene model and **1** will estimate the effects of the nonplanar distortions, while comparison of the CST principal values of this twisted fluoranthene model and **2** will yield substitution effects.

The twist present in **2** occurs primarily at the central benzene ring, with torsion angles around the ring of about 5°. The individual naphthalene moieties in **2** are essentially planar. Compare the calculated CST principal values of C6b of the twisted fluoranthene structure (respective averages of δ_{11}, δ_{22}, and δ_{33} are 226.5, 163.3, and 38.6 ppm) to those for the planar structure of **1** (Table 2). On the basis of the calculated values, the twist strain increases δ_{11} of C6b by 6.3 ppm from 220.2 ppm for **1** to 226.5 ppm for the twisted fluoranthene. The δ_{11} of C6b for the twisted fluoranthene molecule is then decreased by 23.4 ppm from 226.5 to 203.1 ppm by the substitution of the two naphthalene moieties to form **2**. Hence, the net effect of twist and substitution effects between **1** and **2** is −17.1 ppm in the GIAO-B3PW91/D95** data compared to an experimental difference of −20.6 ppm. This suggests that the large change in δ_{11} is mostly due to substitution effects even though the twist effects are quite significant.

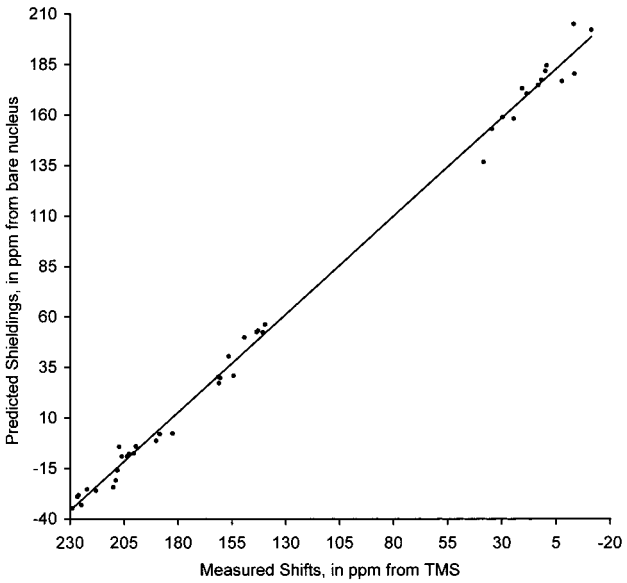

Figure 8. Plot of the GIAO-B3PW91/D95** shieldings vs measured CST principal values. The regression equation used to convert the computed shieldings to the experimental shift scale is $\sigma = -0.97$ (± 0.02) $\delta + 188$ (± 3). Slope and intercept uncertainties are at 95% confidence.

Figure 8 shows a plot of the averaged chemical shieldings of **1** and **2** plotted against the experimental values. The RMS for the predicted values relative to the regression line is 5.6 ppm, which is slightly larger than that reported for other PAHs. For example, in a recent study of biphenylene the RMS was 3.1 ppm[1] and for a series of hetero-substituted aromatic compounds, the RMS was 5.2 ppm.[3] It is not surprising that the present RMS value is larger than these other cases. The considerable spectral overlap observed in this work necessitated averaging some of the predicted principal values. Also, intermolecular effects are not accommodated except for the use of both molecules of **1** in the asymmetric unit. The largest outlier on the plot is the δ_{33} principal value of the C3a in **1**. This particular value showed no improvement between a calculation of a single molecule of **1** (not reported) and the pair of molecules of **1**, suggesting that the error arises from effects other than a lack of accommodating intermolecular interactions.

Conclusions

This work provides additional data on ring strain and other steric effects on the CST principle values for PAHs that contain five-member rings. The expected shift to higher frequency in the δ_{33} component of the principal values of carbons experiencing ring strain is observed for both **1** and **2**. Comparison of **1** and **2** to the hypothetical twisted fluoranthene model suggests that the magnitude of the change in δ_{11} due to substitution effects is about three times that of the twist effects, though the two effects are opposite in sign. Twist strain moves the δ_{11} principal value of an aromatic carbon to higher frequency. In the particular example observed here, there is nevertheless a larger shift to lower frequency due to chemical substitution. The correlation of experimental CST data with theory is of comparable quality to that of previous studies of PAH systems.

Acknowledgment. Support for this work was provided by Basic Energy Sciences, U.S. Department of Energy, through Grant DE-FG03-94ER14452, and by funds provided by the University of Utah as part of the DOE Advanced Strategic Computing Program (ASCI). Computer resources were provided

by the Center for High Performance Computing at the University of Utah. The authors are indebted to Don W. Alderman for many helpful and insightful discussions in the course of this work. The authors thank Dr. Atta M. Arif for his technical assistance in analyzing the literature crystallographic data.

References and Notes

(1) Barich, D. H.; Pugmire, R. J.; Grant, D. M.; Iuliucci, R. J. *J. Phys. Chem. A* **2001**, *105*, 6780−6784.

(2) Barich, D. H.; Orendt, A. M.; Pugmire, R. J.; Grant, D. M. *J. Phys. Chem. A* **2000**, *104*, 8290−8295.

(3) Barich, D. H.; Facelli, J. C.; Hu, J. Z.; Alderman, D. W.; Wang, W.; Pugmire, R. J.; Grant, D. M. *Magn. Reson. Chem.* **2001**, *39*, 115−121.

(4) Orendt, A. M.; Facelli, J. C.; Bai, S.; Rai, A.; Gossett, M.; Scott, L. T.; Boerio-Goates, J.; Pugmire, R. J.; Grant, D. M. *J. Phys. Chem. A* **2000**, *104*, 149−155.

(5) Iuliucci, R. J.; Phung, C. G.; Facelli, J. C.; Grant, D. M. *J. Am. Chem. Soc.* **1998**, *120*, 9305−9311.

(6) Iuliucci, R. J.; Phung, C. G.; Facelli, J. C.; Grant, D. M. *J. Am. Chem. Soc.* **1996**, *118*, 4880−4888.

(7) Iuliucci, R. J.; Facelli, J. C.; Alderman, D. W.; Grant, D. M. *J. Am. Chem. Soc.* **1995**, *117*, 2336−2343.

(8) Alderman, D. W.; McGeorge, G.; Hu, J. Z.; Pugmire, R. J.; Grant, D. M. *Mol. Phys.* **1998**, *95*, 1113−1126.

(9) McGeorge, G.; Hu, J. Z.; Mayne, C. L.; Alderman, D. W.; Pugmire, R. J.; Grant, D. M. *J. Magn. Reson.* **1997**, *129*, 134−144.

(10) Hazell, A. C.; Jones, D. W.; Sowden, J. M. *Acta Crytallogr.* **1977**, *B33*, 1516−1522.

(11) Ho, D. M.; Pascal, R. A., Jr. *Chem. Mater.* **1993**, *5*, 1358−1361.

(12) Orendt, A. M.; Sethi, N. K.; Facelli, J. C.; Horton, W. J.; Pugmire, R. J.; Grant, D. M. *J. Am. Chem. Soc.* **1992**, *114*, 2832−2836.

(13) Buntkowsky, G.; Hoffman, W.; Kupka, T.; Pasterna, G.; Jaworska, M.; Vieth, H.-M. *J. Phys. Chem. A* **1998**, *102*, 5794−5801.

(14) Solum, M. S.; Pugmire, R. J.; Grant, D. M. *Energy Fuels* **1989**, *3*, 187−193.

(15) Hu, J. Z.; Solum, M. S.; Taylor, C. M. V.; Pugmire, R. J.; Grant, D. M. *Energy Fuels* **2001**, *15*, 14−22.

(16) Solum, M. S.; Sarofim, A. F.; Pugmire, R. J.; Fletcher, T. H.; Zhang, H. *Energy Fuels* **2001**, *15*, 961−971.

(17) Barnett, L.; Ho, D. G.; Baldridge, K. K.; Pascal, R. A., Jr. *J. Am. Chem. Soc.* **1999**, *121*, 727−733.

(18) Pines, A.; Gibby, M. G.; Waugh, J. S. *J. Chem. Phys.* **1973**, *59*, 569−590.

(19) Frisch, M. J.; Trucks, G. W.; Schlegel, H. B.; Scuseria, G. E.; Robb, M. A.; Cheeseman, J. R.; Zakrzewski, V. G.; Montgomery, J. A., Jr.; Stratmann, R. E.; Burant, J. C.; Dapprich, S.; Millam, J. M.; Daniels, A. D.; Kudin, K. N.; Strain, M. C.; Farkas, O.; Tomasi, J.; Barone, V.; Cossi, M.; Cammi, R.; Mennucci, B.; Pomelli, C.; Adamo, C.; Clifford, S.; Ochterski, J.; Petersson, G. A.; Ayala, P. Y.; Cui, Q.; Morokuma, K.; Malick, D. K.; Rabuck, A. D.; Raghavachari, K.; Foresman, J. B.; Cioslowski, J.; Ortiz, J. V.; Stefanov, B. B.; Liu, G.; Liashenko, A.; Piskorz, P.; Komaromi, I.; Gomperts, R.; Martin, R. L.; Fox, D. J.; Keith, T.; Al-Laham, M. A.; Peng, C. Y.; Nanayakkara, A.; Gonzalez, C.; Challacombe, M.; Gill, P. M. W.; Johnson, B. G.; Chen, W.; Wong, M. W.; Andres, J. L.; Head-Gordon, M.; Replogle, E. S.; Pople, J. A. *Gaussian 98*, revision A.7; Gaussian, Inc.: Pittsburgh, PA, 1998.

(20) London, F. *J. Phys. Radium* **1937**, *8*, 397.

(21) Perdew, J. P.; Wang, Y. *Phys. Rev. B* **1992**, *45*, 13244−13249.

(22) Ditchfield, R. *Mol. Phys.* **1974**, *27*, 789−807.

(23) Becke, A. D. *J. Chem. Phys.* **1993**, *98*, 5648−5652.

(24) Lee, C.; Yang, W.; Parr, R. G. *Phys. Rev. B* **1988**, *37*, 785−789.

(25) Dunning, T. H., Jr. *J. Chem. Phys.* **1989**, *90*, 1007−1023.

(26) Wolinski, K.; Hinton, J. F.; Pulay, P. *J. Am. Chem. Soc.* **1990**, *112*, 8251−8260.

(27) Cheeseman, J. R.; Trucks, G. W.; Keith, T. A.; Frisch, M. J. *J. Chem. Phys.* **1996**, *104*, 5497−5509.

(28) Rauhut, G.; Puyear, S.; Wolinski, K.; Pulay, P. *J. Phys. Chem.* **1996**, *100*, 6310−6316.

(29) Liu, F.; Phung, C. G.; Alderman, D. W.; Grant, D. M. *J. Magn. Reson.* **1996**, *120*, 231−241.

(30) Alderman, D. W.; Sherwood, M. H.; Grant, D. M. *J. Magn. Reson.* **1993**, *101*, 188−197.

(31) Ernst, L. *Org. Magn. Reson.* **1976**, *8*, 161.

(32) Johnston, M. D.; Martin, G. E. Castle, R. N. *Spectrosc. Lett.* **1988**, *21*, 853−857.

(33) Sherwood, M. H.; Facelli, J. C.; Alderman, D. W.; Grant, D. M. *J. Am. Chem. Soc.* **1991**, *113*, 750−753.